SF newsletter 342 #13-18

M. Momose (Ibaraki Univ.)

#15, 16 (Yebes 40m/IRAM 30m望遠鏡による
30-50GHz & 77-240GHzのラインサーベイの結果)

#14 (ちょっとだけ紹介)

その他 (アブストラクトと一言メモ)

15.

Discovery in space of ethanolamine, the simplest phospholipid head group

Víctor M. Rivilla, Izaskun Jiménez-Serra, Jesús Martín-Pintado, Carlos Briones, Lucas F. Rodríguez-Almeida, Fernando Rico-Villas, Belén Tercero, Shaoshan Zeng, Laura Colzi, Pablo de Vicente, Sergio Martín, Miguel A. Requena-Torres ★ Cell membranes are a key element of life because they keep the genetic material and metabolic machinery together. All present cell membranes are made of phospholipids, yet the nature of the first membranes and the origin of phospholipids are still under debate. We report here the first detection in space of ethanolamine, $NH_2CH_2CH_2OH$, which forms the hydrophilic head of the simplest and second most abundant phospholipid in membranes. The molecular column density of ethanolamine in interstellar space is N=(1.51±0.07)×10^{13} cm^{-2}, implying a molecular abundance with respect to H_2 of (0.9-1.4)×10^{-10}. Previous studies reported its presence in meteoritic material but they suggested that it is synthesized in the meteorite itself by decomposition of amino acids. However, we find that the proportion of the molecule with respect to water in the interstellar medium is similar to the one found in the meteorite (10^{-6}). These results indicate that ethanolamine forms efficiently in space and, if delivered onto early Earth, it could have contributed to the assembling and early evolution of primitive membranes.

- **Sgr N2領域にあるマイルドなcloud-cloud collision領域G+0.693-0.027に対する Yebes 40m (31.0-50.4GHz) + IRAM 30m (71.77-116.72GHz)のラインサーベイで，メタノールアミンの星間空間での初検出**
- **メタノールアミンは生命体にとって欠かせない，細胞膜やコンパートメントを形作る「リン脂質」の中の親水性頭部として最も多く含まれるものの1つ**
- **N= 1.5×10^{13} cm^{-2}, H_2に対する相対アバンダンスは(0.9-1.4)×10^{-10}。**
- **メタノールアミンはエンスタタイトコンドライト隕石でも見つかっていたが，H_2Oに対する存在比はそれと同程度だった。水とともに，地球に運ばれてきたかも！？**

生命体の3つの基本サブシステム

- Compartment (コンパートメント＝膜で区画された構成。例えば細胞膜)
- Metabolic machinery（代謝システム）
- Information-bearing molecules （遺伝情報を格納する分子）

後ろの2つは compartmentがあって始めて成り立つものであるので,
細胞膜をはじめとするCompartmentは最初の生命体の発現とその後の進化の必須条件と言える

細胞膜の特徴と
エタノールアミン

リン脂質(phospholipid)が２重構造を作り
脂溶性のものは透過させるのに対して
水溶性のものはほとんど透過しない

リン脂質は親水性頭部(hydrophilic head)
と疎水性尾部(hydrophobic tails)からなる

エタノールアミンは，細胞膜リン脂質の
親水性頭部の中で最も簡単な構造を持ち，
かつ細胞膜で2番目に多いリン脂質
(ホスファチジルエタノールアミン)を作る

エタノールアミン($NH_2CH_2CH_2OH$)は，
グリシン(NH_2CH_2COOH)の前駆体
としても有望視されている

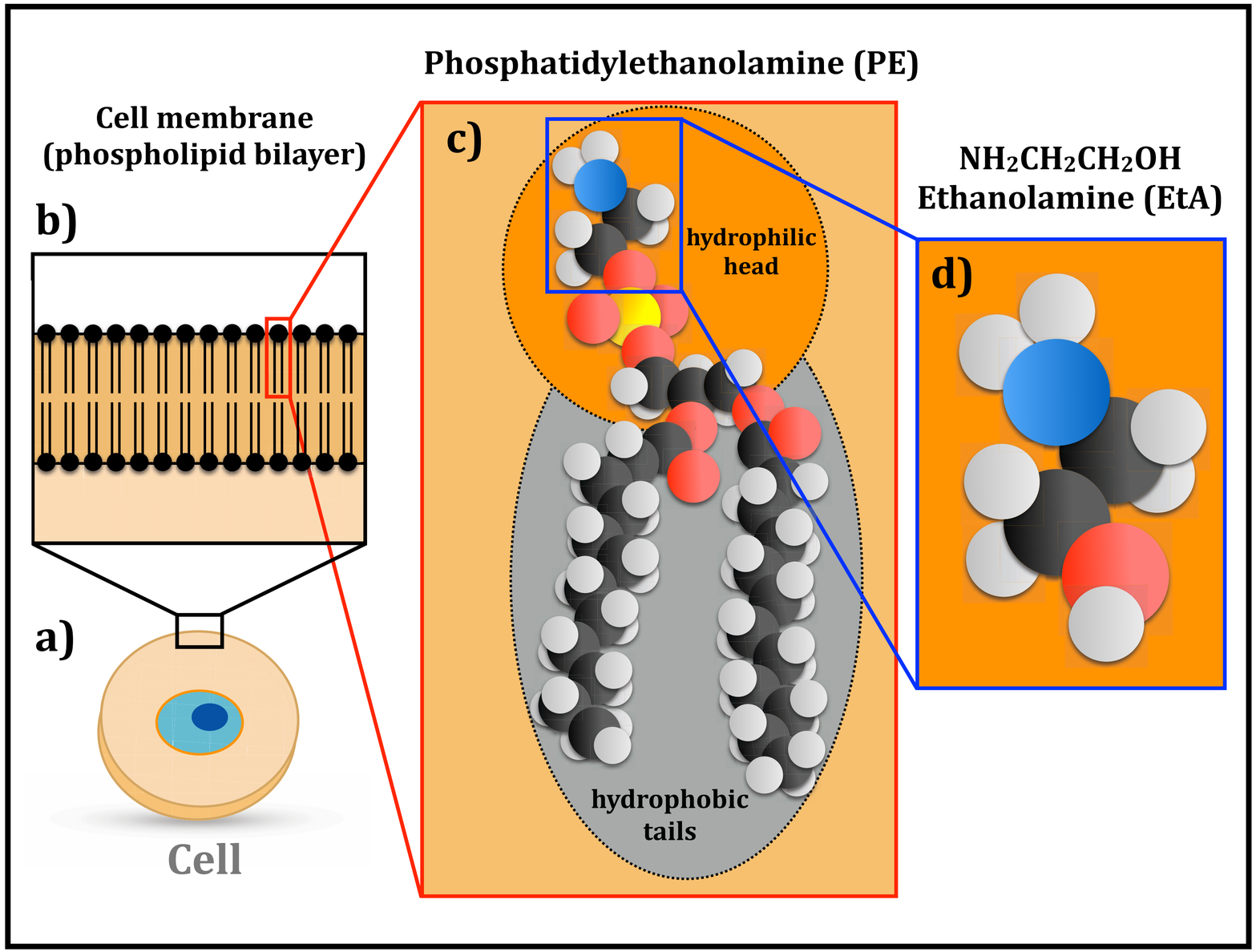

宇宙物質中での
エタノールアミン(EtA)

アルマハータ・シッタ隕石はEtAを含むが
その起源は不明であった。隕石母天体での
特殊環境下でのアミノ酸分解？　それだと
原始地球への供給量は限られる

別の可能性：EtAがISMで形成される
今回，Yebes 40mとIRAM 30mを用いた
ラインサーベイで初検出！

観測対象のG+0.693-0.027: Sgr N2領域に
ある，マイルドなCCCに伴う低速(<20km)
ショックを伴う分子雲。アイスマントルの
erosionによる豊富なガス化学。密度~10^4 cm^{-3}オーダ，T_{ex} = 5-15Kでラインの密度
(blending)は控え目→探索には理想的。

観測帯域中にあると計算されていた全遷移 (23,655本!)のうち
強いと予想されていた45本中，ブレンドしていない検出が14本

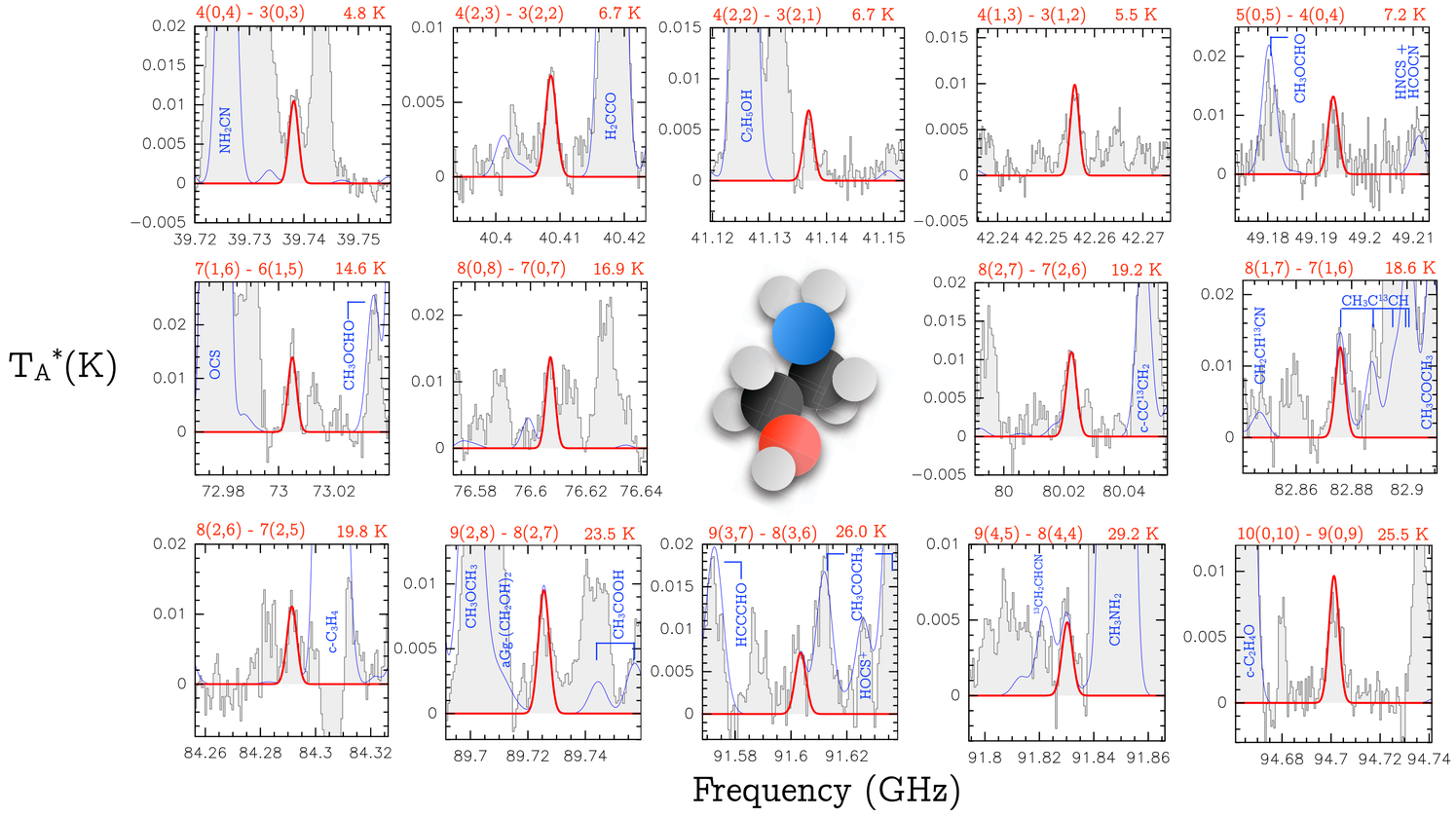

Fig. 2. Unblended or slightly blended transitions of EtA towards the G+0.693-0.027 molecular cloud. The quantum numbers involved in the transition are indicated in the upper left of each panel, and the energies of the upper level are indicated in the upper right. The red thick line depicts the best LTE fit to the EtA rotational transitions. The thin blue line shows the expected molecular emission from all the molecular species identified in our spectral survey, overplotted to the observed spectra (gray histograms). The three-dimensional structure of EtA is shown in the center of the figure: black, red, blue and white balls denote carbon, oxygen, nitrogen and hydrogen atoms, respectively.

赤がEtA，青は全分子を考慮した予想スペクトル，
結構よく合っている！

ブレンドしていない遷移の一覧

Table 1. Spectroscopic information (rest frequency, Einstein coefficients (A_{ul}), and energy of the upper levels (E_{up}) of the 14 unblended or slightly blended rotational transitions of EtA detected towards the G+0.693 molecular cloud (shown in Fig. 2).

Frequency (GHz)	Transition	logA_{ul} (s^{-1})	E_{up} (K)
39.7379429	4(0,4) - 3(0,3)	-5.64603	4.8
40.4083769	4(2,3) - 3(2,2)	-5.74549	6.7
41.1366268	4(2,2) - 3(2,1)	-5.72208	6.7
42.2557255	4(1,3) - 3(1,2)	-5.59088	5.5
49.1932727	5(0,5) - 4(0,4)	-5.35979	7.2
73.0048603	7(1,6) - 6(1,5)	-4.84093	14.6
76.6071016	8(0,8) - 7(0,7)	-4.76916	16.9
80.0223886	8(2,7) - 7(2,6)	-4.73500	19.2
82.8757878	8(1,7) - 7(1,6)	-4.67140	18.6
84.2912932	8(2,6) - 7(2,5)	-4.66443	19.8
89.7254251	9(2,8) - 8(2,7)	-4.57750	23.5
91.6032870	9(3,7) - 8(3,6)	-4.57780	26.0
91.8301065	9(4,5) - 8(4,4)	-4.61854	29.2
94.7010488	10(0,10) - 9(0,9)	-4.48695	25.5

観測帯域中にあると計算されていた全遷移 (23,655本!)のうち

強いと予想されていた45本中，ブレンドしていない検出が14本

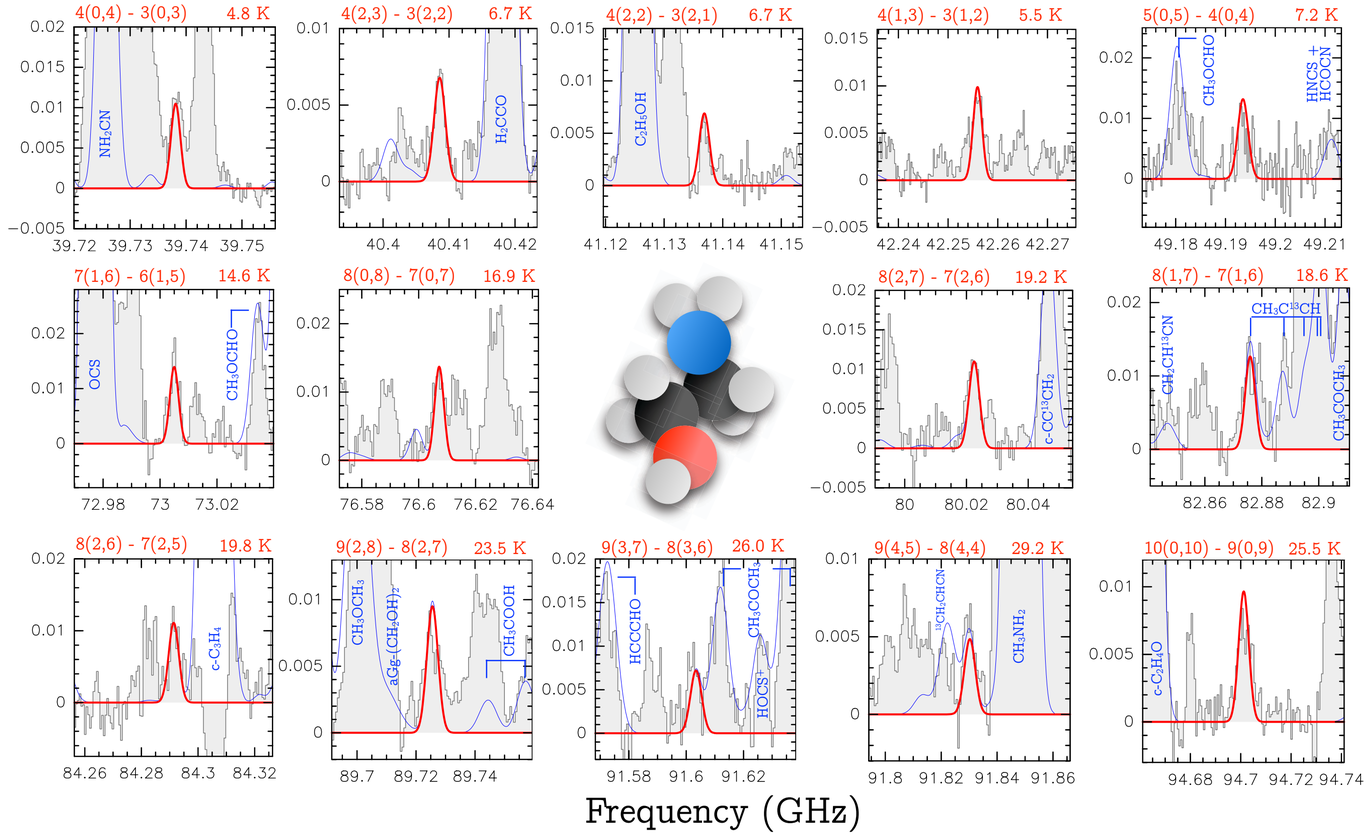

Fig. 2. Unblended or slightly blended transitions of EtA towards the G+0.693-0.027 molecular cloud. The quantum numbers involved in the transition are indicated in the upper left of each panel, and the energies of the upper level are indicated in the upper right. The red thick line depicts the best LTE fit to the EtA rotational transitions. The thin blue line shows the expected molecular emission from all the molecular species identified in our spectral survey, overplotted to the observed spectra (gray histograms). The three-dimensional structure of EtA is shown in the center of the figure: black, red, blue and white balls denote carbon, oxygen, nitrogen and hydrogen atoms, respectively.

赤がEtA，青は全分子を考慮した予想スペクトル

(SLIMによる)，結構よく合っている！

ブレンドしている遷移が31本

全speciesを含めて計算したモデルと大きな矛盾なし

↓

確かにEtA起源

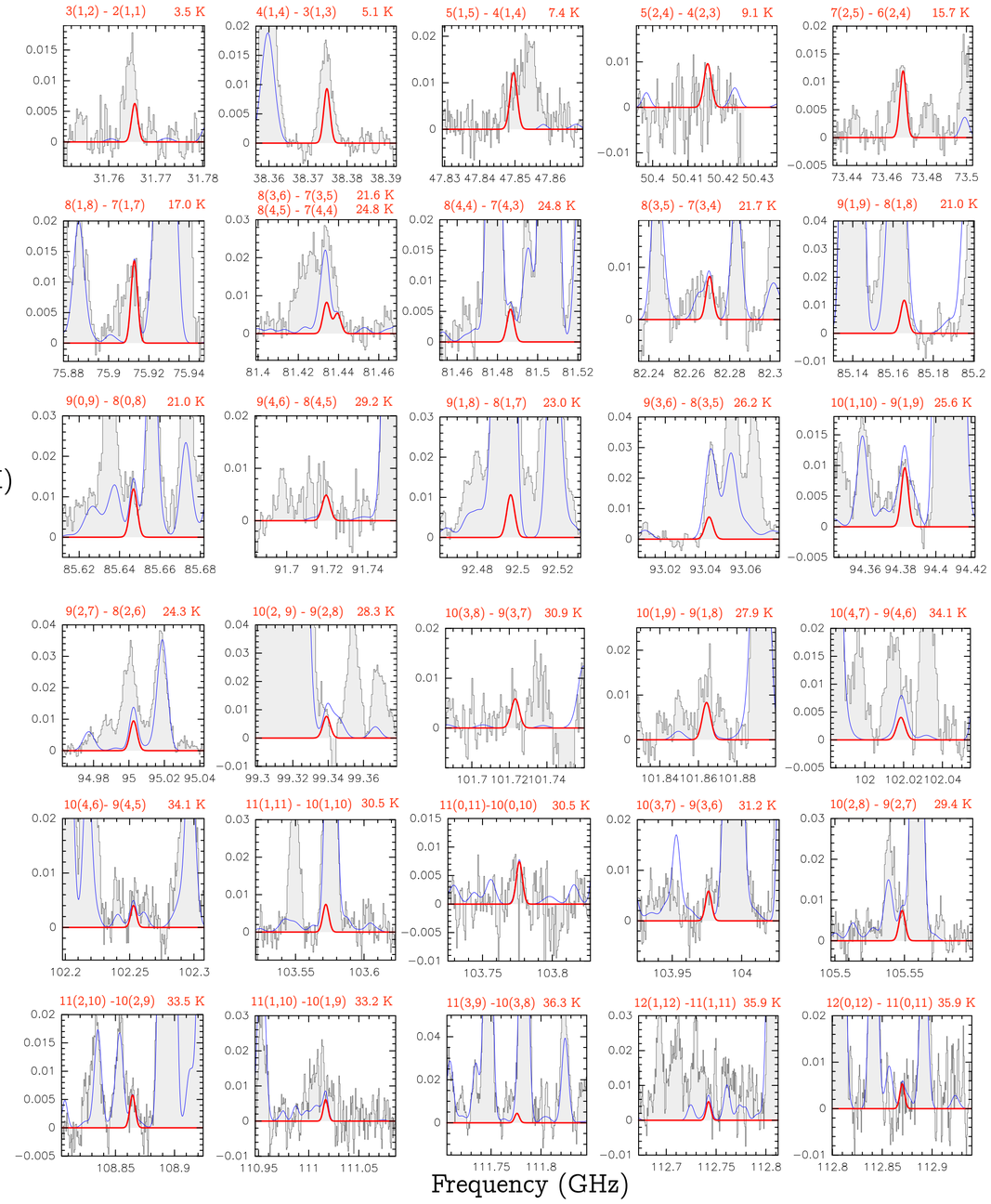

Fig. 3. Transitions of ethanolamine that appear blended in the observed spectra of G+0.693. All of them have line intensities $>$ 5 mK, according to the best LTE fit described in the text. The quantum numbers involved in the transition are indicated in the upper left of each panel, and the energies of the upper level are indicated in the upper right. The red thick line depicts the best LTE fit obtained fitting the EtA rotational transitions shown in Fig. 2. The thin blue line shows the predicted molecular emission from all the molecular species identified in our spectral survey, overplotted to the observed spectra (gray histograms).

ブレンドしてない遷移に対するRotation Diagram

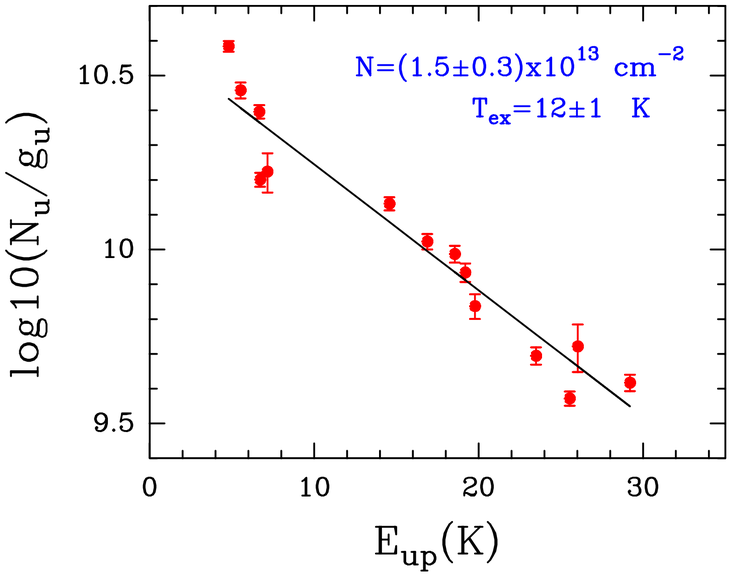

Fig. 4. Rotational diagram of EtA. The analysis procedure is described in the Materials and Methods section. The red dots correspond to the 14 EtA transitions shown in Fig. 2 and Table 1. The black line is the best linear fit to the data points. The derived values for the molecular column density (N) and the excitation temperature ($T_{\rm ex}$), along with their uncertainties, are indicated in blue in the upper right corner.

C^{18}Oから求めたH$_2$柱密度との比較

X(EtA) (0.9-1.4)x10^{-10}：結構高い。

H$_2$Oに対する存在比は隕石と同レベル，星間空間に豊富に存在？

星間空間でのEtA形成反応の候補

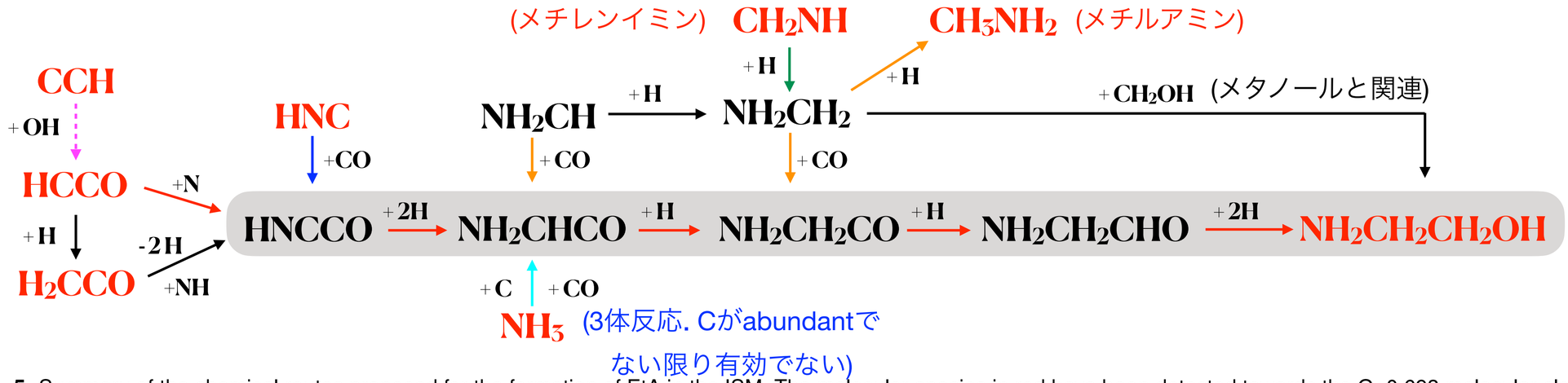

Fig. 5. Summary of the chemical routes proposed for the formation of EtA in the ISM. The molecular species in red have been detected towards the G+0.693 molecular cloud. The gray shaded area corresponds to a hydrogenation chain. The chemical reactions indicated with colored arrows have been proposed in previous works: magenta (36), blue (38), orange (41), cyan (39), green (41, 47). In black, we show the formation routes proposed in this work. The solid arrows indicate surface chemistry reactions, and dashed arrows denote gas phase chemistry.

- （先行研究）HNCCOのダスト表面上でのH付加がほぼ唯一の提案（グレー部分）。
- HNCCOは，(i) HCCOにNが付加する反応か，(ii)H_2CCOのダスト表面反応のいずれかで作る。
  HCCOはG+0.693でもtentativeに検出されている(次頁)他，他にcold dark cloudsで検出報告あり。
- （新たな提案）NH_2CH_2にCH_2OHを付加して作るのもありうるのでは？
- グレーの経路中にある分子の大部分は検出できそうな回転遷移は知られていないが，EtA直前の
  NH_2CH_2CHOは理論計算による回転遷移周波数の値あり(観測には実験室分光による精密化が必要)。
  反応経路を決定するために，今後有望な探索対象になるかも。

Tentative detection of HCCO (ketenyl)

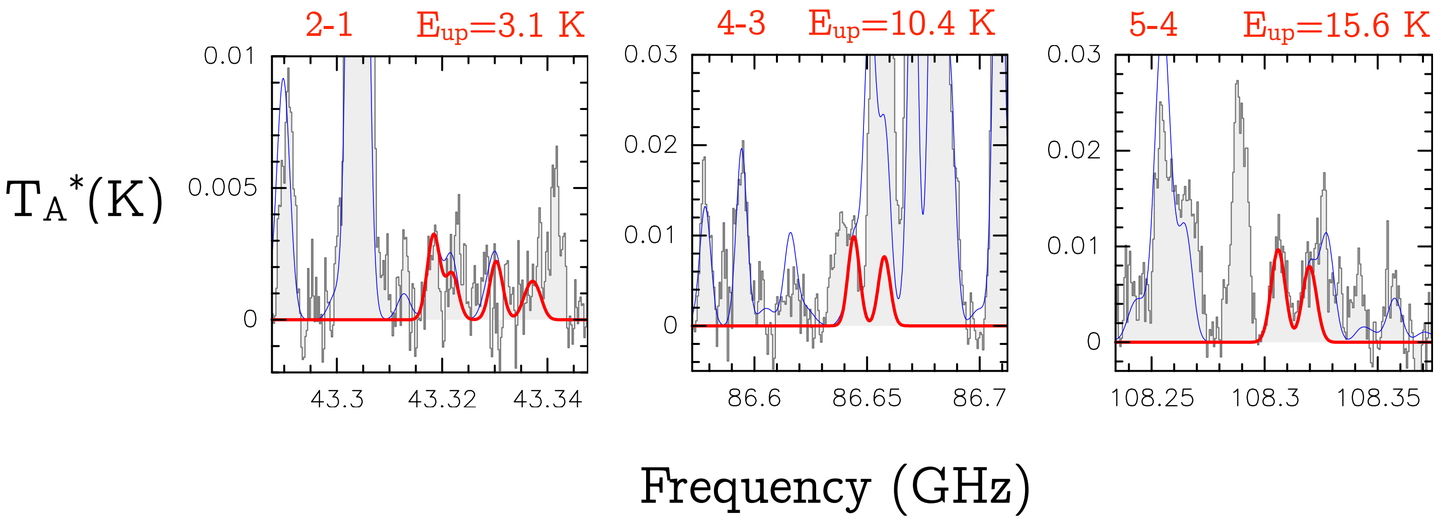

Fig. 6. Transitions of HCCO tentatively identified in the spectra of G+0.693. The rotational quantum numbers involved in the transition are indicated in the upper left of each panel, and the energies of the upper level are indicated in the upper right. The red thick line depicts the LTE synthetic spectrum of HCCO. The blue thin line shows the predicted molecular emission from all the molecular species identified in our spectral survey, overplotted to the observed spectra (gray histograms).

Table 3. Spectroscopic information (rest frequency, Einstein coefficients ($A_{\rm ul}$), and energy of the upper levels ($E_{\rm up}$) of the rotational transitions of ketenyl (HCCO) tentatively detected towards the G+0.693 molecular cloud (shown in Fig. 6).

Frequency (GHz)	Transition	log$A_{\rm ul}$ (s^{-1})	$E_{\rm up}$ (K)
43.3176674	2(3,3) - 1(2,2)	-6.0192	3.1
43.3211451	2(3,2) - 1(2,1)	-6.1404	3.1
43.3295421	2(2,2) - 1(1,1)	-6.0343	3.1
43.3354627	2(2,1) - 1(1,0)	-6.2739	3.1
43.3368615	2(3,2) - 1(2,2)	-6.6741	3.1
43.3373040	2(2,1) - 1(2,1)	-6.4207	3.1
86.6191857	4(4,3) - 3(3,3)	-6.9202	10.4
86.6423419	4(5,5) - 3(4,4)	-5.0703	10.4
86.6438483	4(5,4) - 3(4,3)	-5.0942	10.4
86.6558306	4(4,4) - 3(3,3)	-5.0772	10.4
86.6574849	4(4,3) - 3(3,2)	-5.1070	10.4
86.6652791	4(5,4) - 3(4,4)	-6.3845	10.4
108.2823800	5(5,4) - 4(4,4)	-6.7293	15.6
108.3040553	5(6,6) - 4(5,5)	-4.7698	15.6
108.3051187	5(6,5) - 4(5,4)	-4.7840	15.6
108.3178903	5(5,5) - 4(4,4)	-4.7747	15.6
108.3190248	5(5,4) - 4(4,3)	-4.7916	15.6
108.3280559	5(6,5) - 4(5,5)	-6.2997	15.6

アルマハータ・シッタ隕石は（ユレイライトに分類されるが）エンスタタイトコンドライトも含む。エンスタタイトコンドライトは「地球の海」の起源として有望視されており，水と共にEtAが原始地球に供給された可能性は十分ある。そうであれば，原始地球を模した実験的研究は，そこからリン脂質が作られうることを既に示しているので，原始生物がどう発現したかのシナリオにも大きな影響があるかもしれない。

16.

Detection of the cyanomidyl radical (HNCN): a new interstellar species with the NCN backbone

V. M. Rivilla, I. Jiménez-Serra, J. García de la Concepción, J. Martín-Pintado, L. Colzi, L. F. Rodríguez-Almeida, B. Tercero, F. Rico-Villas, S. Zeng, S. Martín, M. A. Requena-Torres, P. de Vicente ★ We report here the first detection in the interstellar medium of the cyanomidyl radical (HNCN). Using the Yebes 40m and the IRAM 30m telescopes, we have targeted the doublets of the N=2−1, 4−3, 5−4, 6−5, and 7−6 transitions of HNCN toward the molecular cloud G+0.693-0.027. We have detected three unblended lines of HNCN, these are the N=6−5 doublet and one line of the N=4−3 transition. Additionally we present one line of the N=5−4 transition partially blended with emission from other species. The Local Thermodynamic Equilibrium best fit to the data gives a molecular abundance of $(0.91\pm0.05)\times10^{-10}$ with respect to H_2. The relatively low abundance of this species in G+0.693-0.027, and its high reactivity, suggest that HNCN is possibly produced by gas-phase chemistry. Our work shows that this highly reactive molecule is present in interstellar space, and thus it represents a plausible precursor of larger prebiotic molecules with the NCN backbone such as cyanamide (NH_2CN), carbodiimide (HNCNH) and formamidine (NH_2CHNH).

アデニン
（核酸塩基の一つ）

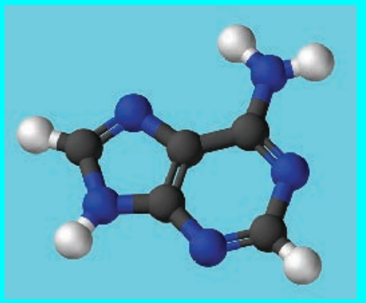

・同様のデータ(124.8-175.5GHz, 223.3-238.3GHzも)から，HNCNの初の明確な検出を議論。

・NCN骨格は，RNAやDNAなどの二重らせん構造を作る核酸塩基(nucleobase)に含まれる基本構造。

・NH_2CN（cyanamide），HNCNH（carbodiimide），NH_2CONH_2（urea, 尿素）はISMで検出例あり。

・HNCNはNCN骨格を持つより簡単な分子であるにもかかわらず，明確な検出例はなかった（実験室分光は Yamamoto & Saito 1994; 当時の天体観測では検出に至らず)。

・今回はG+0.693-0.027で検出した。

今回の検出

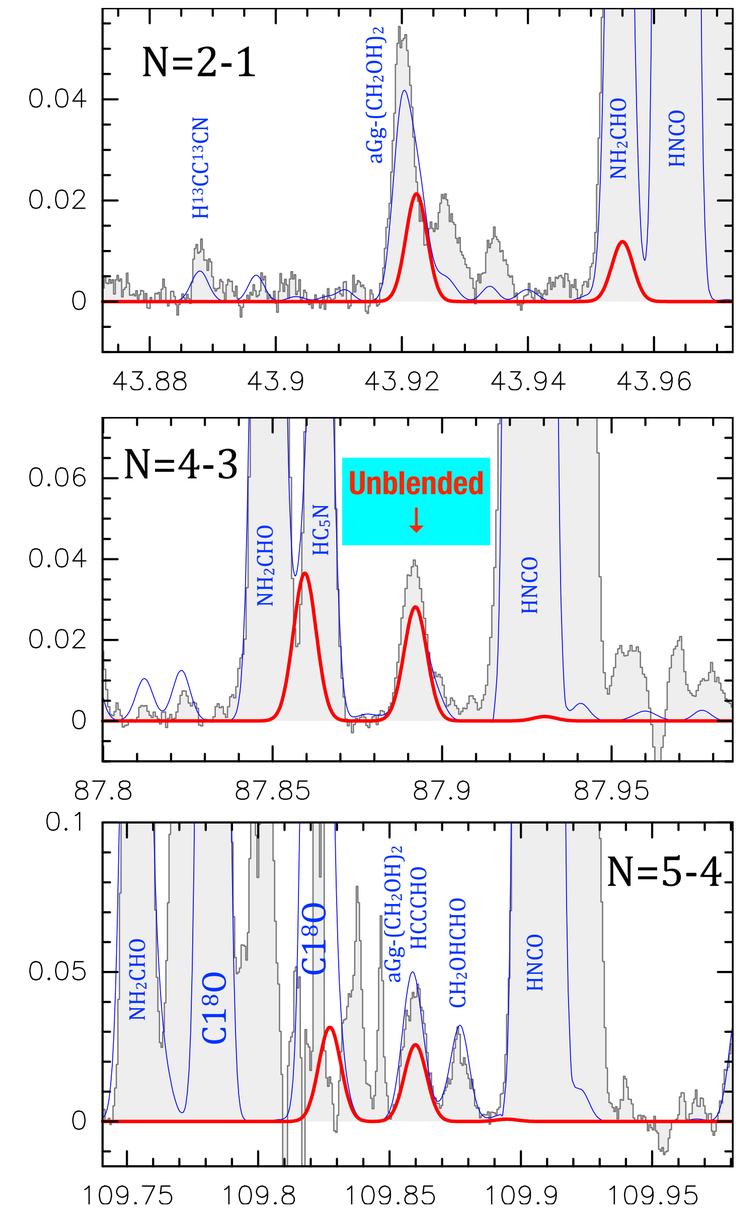

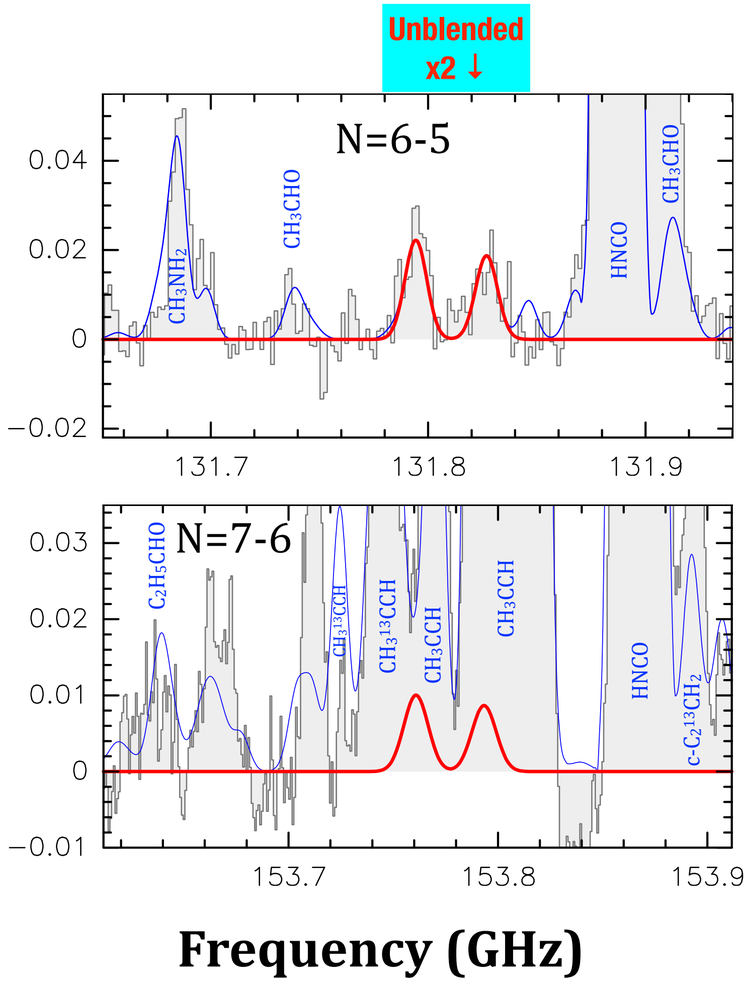

Figure 1. Transitions of HNCN detected in the observed spectra of G+0.693. The best LTE fit to the HNCN lines is shown in red, while the total contribution, including other molecular species (labelled) identified in the region is shown in blue.

※JはN原子のスピンによる微細構造分裂を考慮した角運動量

Table 1. List of observed transitions of HNCN. We provide the parameters from the CDMS catalog entry 041507: frequencies, quantum numbers, and upper state degeneracy (g_u). We also show the values of the base 10 logarithm of the Einstein coefficients (log A_{ul}), and the energy of the upper levels (E_u). The last column indicates the molecular species that produces blending with some HNCN transitions.

Frequency (GHz)	Transition ($N_{K,k,J}$)	log A_{ul} (s^{-1})	g_u	E_u (K)	Blending
43.9225164*	$2_{0,2,5/2}-1_{0,1,3/2}$	-5.688	6	3.2	aGg-$(CH_2OH)_2$
43.9552012	$2_{0,2,3/2}-1_{0,1,1/2}$	-5.7663	4	3.2	NH_2CHO
87.8601563	$4_{0,4,9/2}-3_{0,3,7/2}$	-4.739	10	10.5	HC_5N
87.8927924*	$4_{0,4,7/2}-3_{0,3,5/2}$	-4.7543	8	10.5	unblended
109.8281277	$5_{0,5,11/2}-4_{0,4,9/2}$	-4.4385	12	15.8	$C^{18}O$
109.8607271*	$5_{0,5,9/2}-4_{0,4,7/2}$	-4.4479	10	15.8	aGg-$(CH_2OH)_2$, HCCCHO
131.7953263*	$6_{0,6,13/2}-5_{0,5,11/2}$	-4.1943	14	22.1	unblended
131.8278808*	$6_{0,6,11/2}-5_{0,5,9/2}$	-4.2006	12	22.1	unblended
153.7615965	$7_{0,7,15/2}-6_{0,6,13/2}$	-3.9886	16	29.5	$CH_3^{13}CCH$, CH_3CCH
153.7940979	$7_{0,7,13/2}-6_{0,6,11/2}$	-3.9932	14	29.5	CH_3CCH

* Transitions used to perform the fit with the SLIM-AUTOFIT tool of MADCUBA (see text).

Blendしているのが多いが,

N=4-3の一本と

N=6-5の二本が孤立していて

検出は確か！

赤がHNCN, 青は全分子を考慮した予想スペクトル(SLIM)

Blendが激しくない遷移とN=2-1を組み合わせたLTE解析

Table 2. Derived physical parameters of HNCN and other molecular species that might be chemically related.

Molecule	N ($\times10^{13}$ cm^{-2})	T_{ex} (K)	v_{LSR} (km s^{-1})	$FWHM$ (km s^{-1})	Abundance[a] ($\times10^{-10}$)	Ref.[b]
HNCN	1.2±0.1	8.7±0.7	71±1	25	0.91±0.05	(1)
HNCNH	<2.5	8	69	25	<1.9	(1)
NH_2CN[c]	27±2	6.8±0.2	67±1	24±1	23.0	(2)

(a) We adopted N_{H_2}=(1.4±0.3)$\times10^{23}$ cm^{-2}, from Martín et al. (2008). (b) References: (1) This work; (2) Zeng et al. (2018); (c) N, v_{LSR} and $FWHM$ of the para species; the abundance corresponds to the sum of the ortho and para species.

←$6_{1,6}$ - $7_{0,7}$@223.8GHzが未検出，T_{ex}=8Kを仮定

議論(1)：HNCNの形成過程

- G+0.693-0.027はマイルドなショック領域，アイルマントルのerosionがHNCNの比較的高いアバンダンスと関連している可能性大（広がったSiOも受かっている）
- ダスト表面反応によるHNCN形成は，NCNの水素付加かHNCの窒素付加が提案
- Yamamoto & Saito (1994)ではNH_2CNH^+のe⁻付加を提案。高い反応効率。
- CNとNH_2の気相反応も候補。どちらも10^{-8}オーダーのアバンダンスあり。
- NH_2CN（cyanamide）やHNCNH（carbodiimide）の破壊も考えられる。

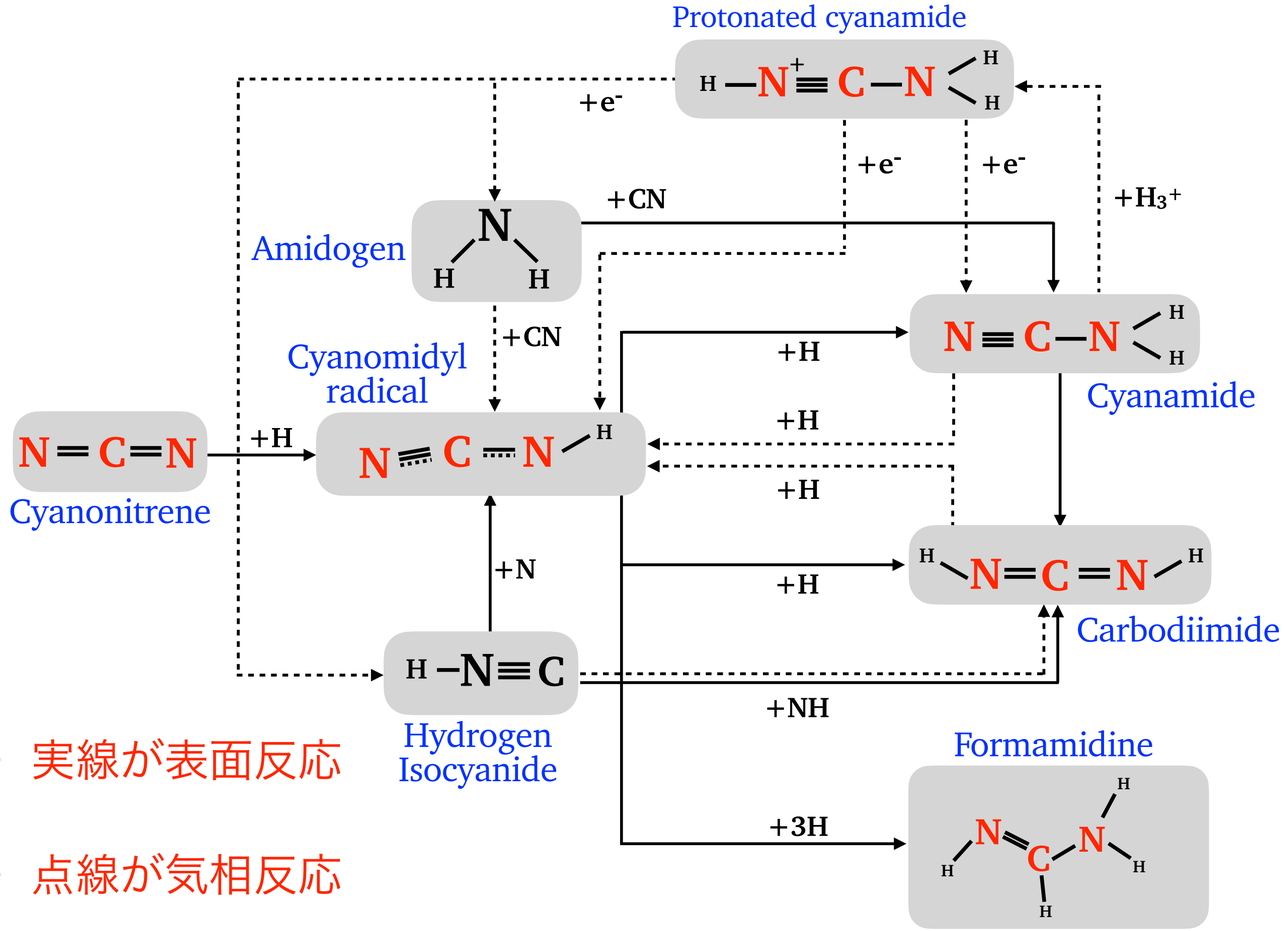

Figure 2. Chemical network for the formation of species with the NCN backbone (highlighted in red) such as the cyanomidyl radical (HNCN), carbodiimide (HNCNH), cyanamide (NH_2CN), protonated cyanamide (NH_2CNH^+) and formamidine (NH_2CHNH). Other chemically related species (the NH_2 radical and HNC) are also indicated. The name of the different molecules are shown in blue. The solid/dashed arrows indicate the surface/gas chemical routes discussed in the text.

議論(2)：HNCN as precursor of prebiotic species

- NH_2CN（cyanamide）：RNAやDNAのヌクレオチドのkey precursor？ G+0.693では，NH_2CNはHNCNの20倍以上のアバンダンス（2ページ前のTable 2）なので，この形成過程は非常に効率的なのかも。
- HNCNH（carbodiimide）： アミノ酸からペプチド結合を作る際の縮合剤として重要？
  - NH_2CNからの光異性化はUV fieldが非常に強くないと起こらないので，この天体に関してはunlikely。
  - NH_2CNの形成よりは非効率？
- NH_2CHNH（formamidine）：アミノ酸の主要precursor？ (Kitadai & Maruyama 2018)

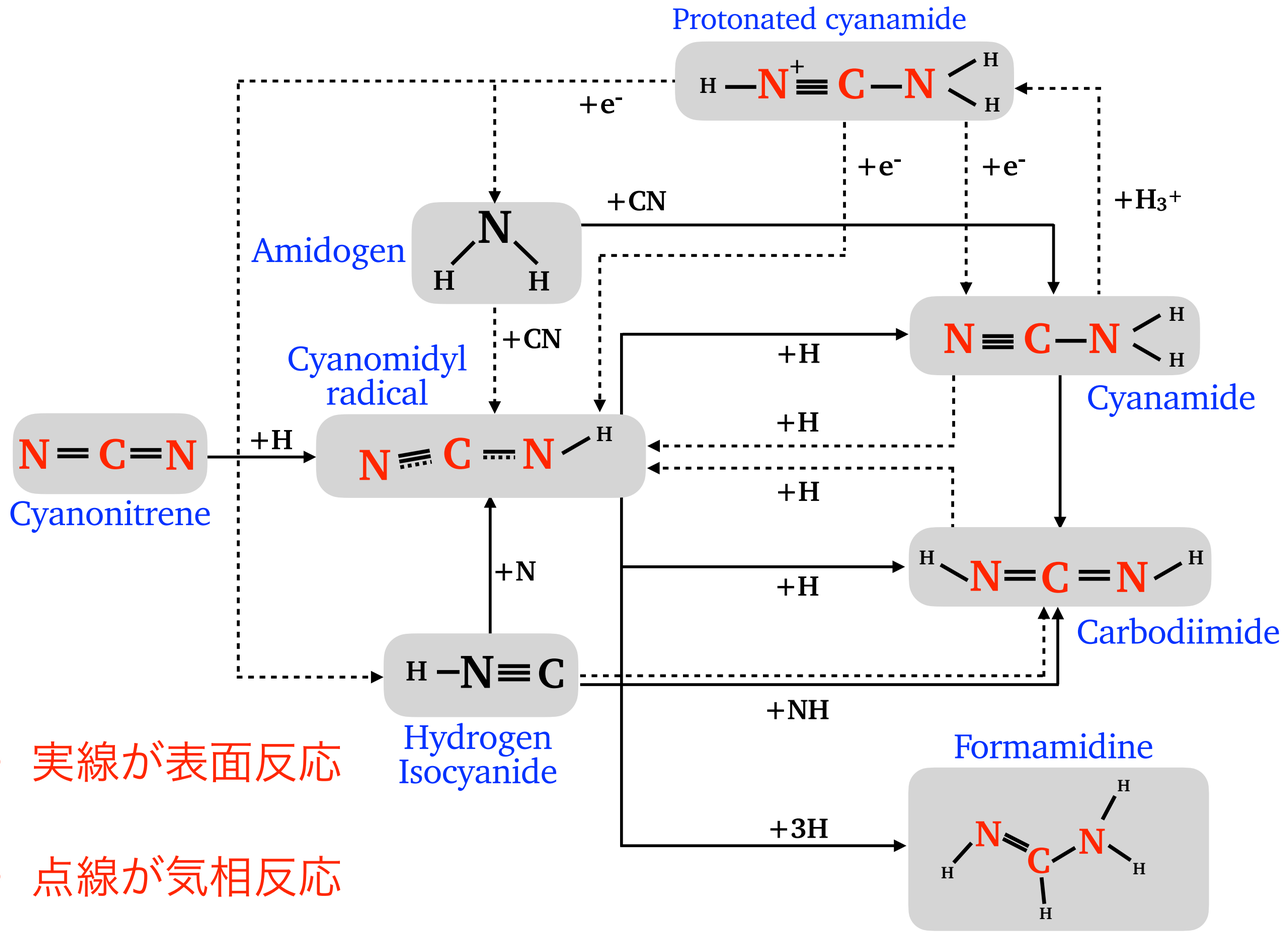

Figure 2. Chemical network for the formation of species with the NCN backbone (highlighted in red) such as the cyanomidyl radical (HNCN), carbodiimide (HNCNH), cyanamide (NH_2CN), protonated cyanamide (NH_2CNH^+) and formamidine (NH_2CHNH). Other chemically related species (the NH_2 radical and HNC) are also indicated. The name of the different molecules are shown in blue. The solid/dashed arrows indicate the surface/gas chemical routes discussed in the text.

14.

Disk Masses and Dust Evolution of Protoplanetary Disks Around Brown Dwarfs

Anneliese M. Rilinger, Catherine C. Espaillat ★ We present the largest sample of brown dwarf (BD) protoplanetary disk spectral energy distributions modeled to date. We compile 46 objects with ALMA observations from four star-forming regions: ρ Ophiuchus, Taurus, Lupus, and Upper Scorpius. Studying multiple regions with various ages enables us to probe disk evolution over time. Specifically, from our models we obtain values for dust grain sizes, dust settling, and disk mass; we compare how each of these parameters vary between the regions. We find that disk mass generally decreases with age, though the youngest region, Ophiuchus, has the lowest disk masses. We find evidence of disk evolution (i.e., grain growth and significant dust settling) in all four regions, indicating that planet formation and disk evolution may begin to occur at earlier stages. We generally find these disks contain too little mass to form planetary companions, though we cannot rule out that planet formation may have already occurred. Finally, we examine the disk mass – host mass relationship and find that BD disks are largely consistent with previously-determined relationships for disks around T Tauri stars.

- D'Alesso によるdisk model(*)を使い，ミリ波・サブミリ波の測光データもあるBrown Dwarfs周りの原始惑星系円盤（46個）に対してSED fitting，円盤の物理量を推定して進化を議論。
  - * 弱い質量降着率を持つ円盤構造をセルフコンシステントに扱えるモデル。
- ダストの成長や赤道面へのダスト沈殿が年齢に応じて進行する傾向を見つけた（というが，ダスト成長については，私にはその妥当性はわからなかった）。
- 円盤質量は惑星を作るほど大きいように見えないが，惑星は既にできているのかも。
- 普通のTタウリ円盤に付随する円盤との質的な違いは見られなかった。

SEDフィットのパラメータ依存性

- $\Sigma \propto \dot{M}\alpha^{-1}$: αが小さいほど同じ$\dot{M}$にするには高いΣが必要
- ε：ダスト沈殿度合いを表すパラメータ，小さいほどより沈殿，ダストが成長
- ミリ波と遠赤外線の測光が両方無いと，縮退が解けない

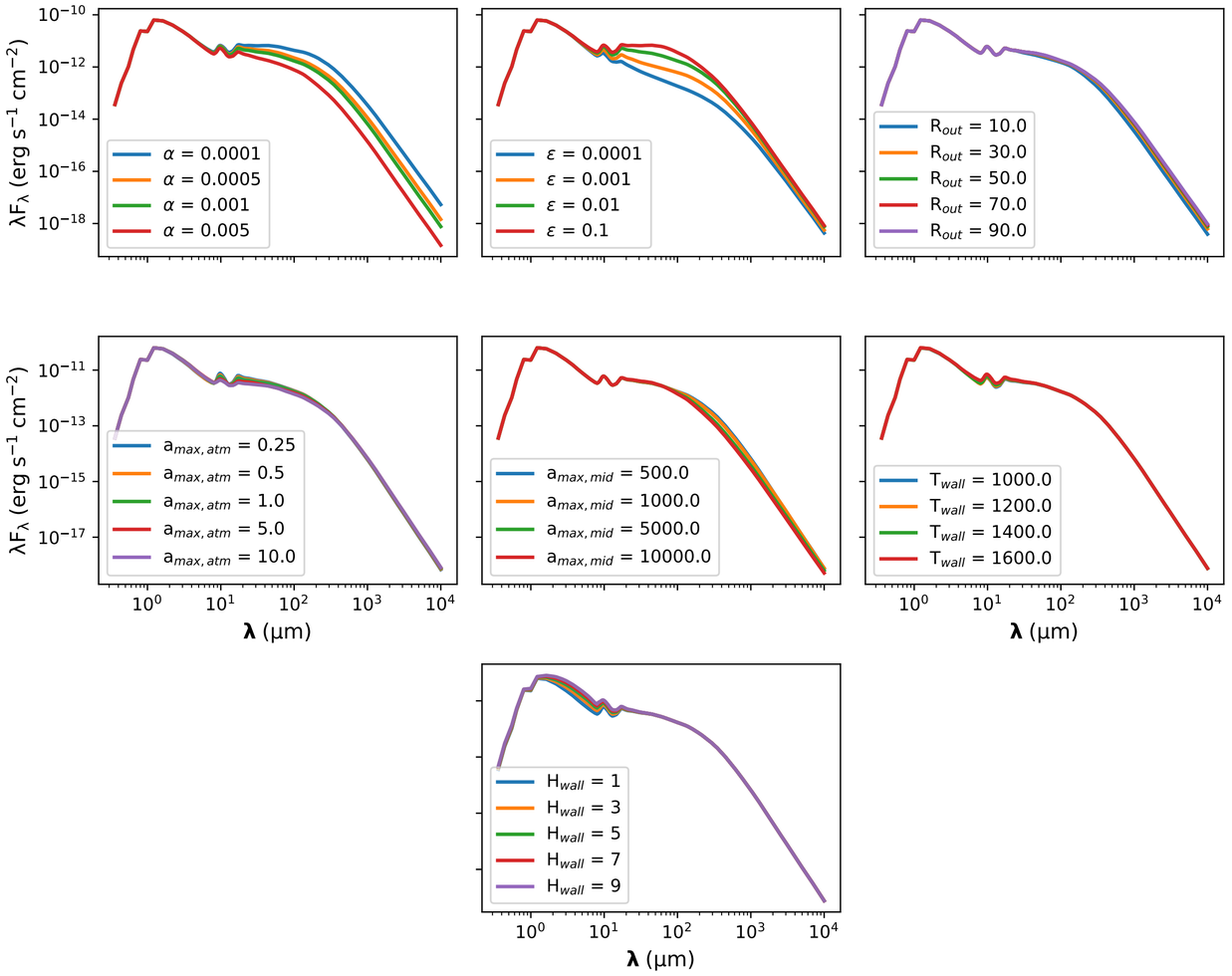

Figure 1. Effect of different parameters in the DIAD SED models. In each panel, all but one parameter is held constant. See text for the values of the fixed parameters.

主要な結果

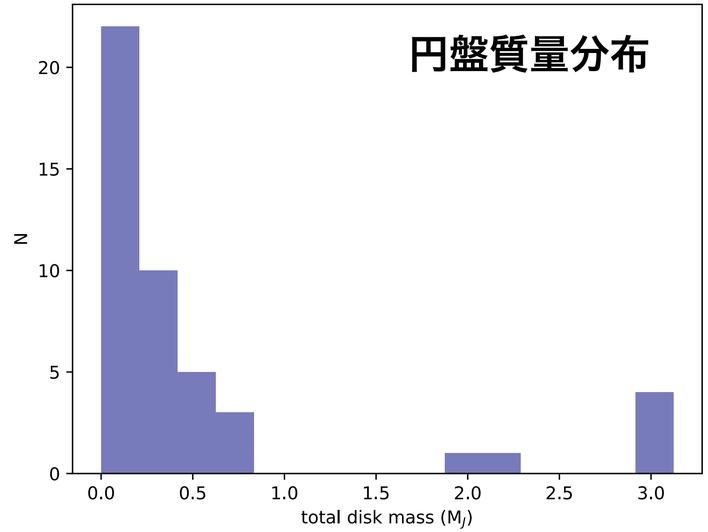

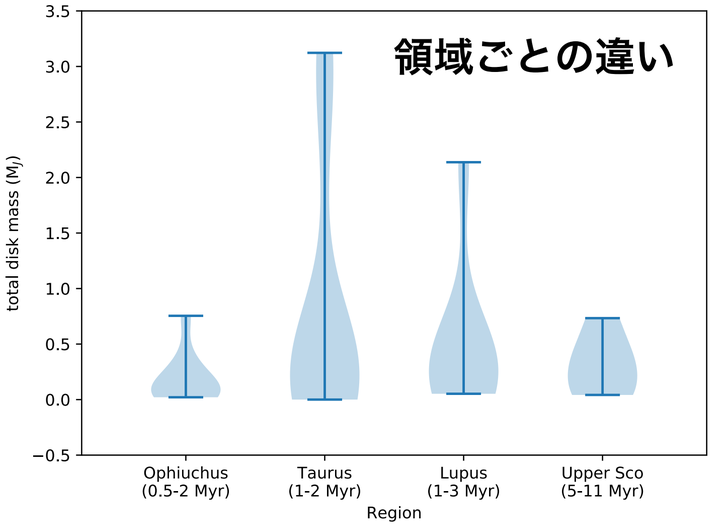

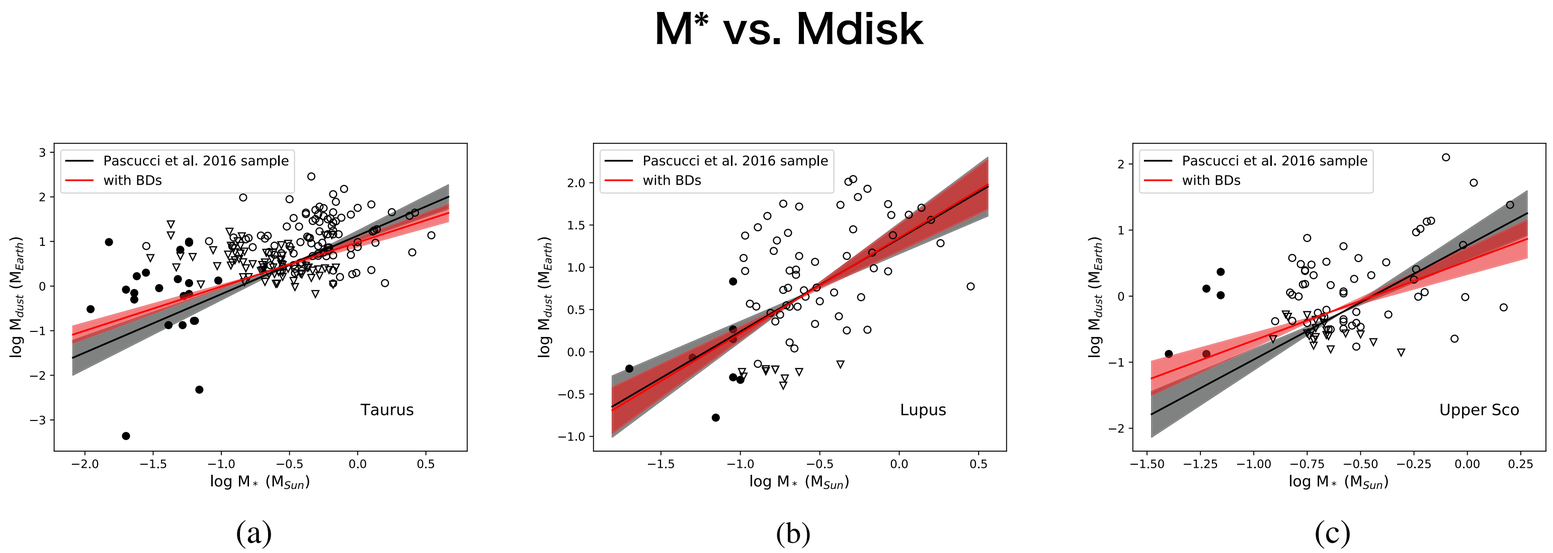

Figure 11. M_{disk} versus M_* relationships for disks in (a) Taurus, (b) Lupus, and (c) Upper Sco. Open circles represent the sample reported in Pascucci et al. (2016), filled circles represent the BDs studied in this work. The black line and grey shaded region represent the best linear fit and uncertainties for the Pascucci et al. (2016) sample; the red line and red shaded region represent the best linear fit and uncertainties for the Pascucci et al. (2016) sample plus the BDs studied in this work. Note that some BDs have very similar host and disk masses, so their points overlap completely.

13.

Census of High- and Medium-mass Protostars V. CO Abundance and the Galactic $X_{\rm CO}$ Factor

Rebecca L. Pitts, Peter J. Barnes ★
We present the second dust continuum data release in the Census of High- and Medium-mass Protostars (CHaMP), expanding the methodology trialed in Pitts et al. 2019 to the entire CHaMP survey area ($280^\circ < l < 300^\circ$, $-4^\circ < b < +2^\circ$). This release includes maps of dust temperature (T_d), H_2 column density (N_{H_2}), gas-phase CO abundance, and temperature-density plots for every prestellar clump with Herschel coverage, showing no evidence of internal heating for most clumps in our sample. We show that CO abundance is a strong function of T_d, and can be fit with a second-order polynomial in log-space, with a typical dispersion of a factor of 2–3. The CO abundance peaks at $20.0^{+0.4}_{-1.0}$ K with a value of $7.4^{+0.2}_{-0.3} \times 10^{-5}$ per H_2; the low T_d at which this maximal abundance occurs relative to laboratory results is likely due to interstellar UV bombardment in the largest survey fields. Finally, we show that, as predicted by theoretical literature and hinted at in previous studies of individual clouds, the conversion factor from integrated ^{12}CO line intensity ($I_{^{12}CO}$) to N_{H_2}, the X_{CO}-factor, varies as a broken power-law in $I_{^{12}CO}$ with a transition zone between 70 and 90 K km^{-1}. The X_{CO}-function we propose has $N_{H_2} \propto I_{^{12}CO}^{0.51}$ for $I_{^{12}CO} \lesssim 70$ K km^{-1} and $N_{H_2} \propto I_{^{12}CO}^{2.3}$ for $I_{^{12}CO} \gtrsim 90$ K km^{-1}. The high-$I_{^{12}CO}$ side should be generalizable with known adjustments for metallicity, but the influence of interstellar UV fields on the low-$I_{^{12}CO}$ side may be sample specific. We discuss how these results expand upon previous works in the CHaMP series, and help tie together observational, theoretical, and laboratory studies on CO over the past decade.

- **Carina-Sagittarius Armに存在する300のclump- to core-scale (~1 - 0.1 pc) condensations対象にしたMopraによる包括的な分子輝線サーベイ**
- **この論文ではCOアバンダンスの変化やXcoを議論**

17.

The dipper population of Taurus seen with K2

Noemi Roggero, Jérôme Bouvier, Luisa M. Rebull, Ann Marie Cody ★ Dippers are typically low-mass, pre-main-sequence stars that display dips in their light curves. These dips have been attributed to dusty warps that form in the inner part of the disk. Our goal is to derive the properties of dipper stars in Taurus to assess the physical mechanisms that induce dipper light curves. We used the light curves of K2 C4 and C13 to select a dipper sample among 179 members and possible members of the Taurus star-forming region based on the light-curve morphology. We studied the periodicities by combining periodograms with wavelet analysis and derived the stellar parameters from the photometry. We also studied the morphology of the photometric dips. We find a dipper occurrence of 30% in disk-bearing stars observed with K2 that were identified visually by us. This represents a lower limit to their true occurrence. About half of the dippers are aperiodic, and most of these are dominated by another type of variability. The chosen sample is of late spectral type (K/M), low mass and moderate mass accretion rates and has periods of a few days. We observed a transient dipper over a few rotation cycles and a dipper with a changing period. The structure of the dips can be complex and varies strongly over timescales of down to one stellar rotation. The corotation radii are located at a few stellar radii, and the temperatures at corotation allow dust survival. Many of the systems are seen at moderate to high inclination. We find that the angular extension of the dusty structure producing the dips is correlated with the stellar period. Magnetospheric accretion, which causes an accretion column and its base to occult the star, can explain most of the observed light curves. Although compatible with the model, many of the stellar inclination angles are moderate and do not exclude mechanisms other than the occultation by an inner disk warp to account for dipper light curves.

- **Taurus領域の若いK/M型星179個に対して，K2データを解析，dipper現象を探索。**
- **Diskを付随する天体の30%からdipper的な変動を発見した。**
- **Dipのパターンは複雑で星の自転周期と同等な時間スケールまで変化が見られる。**
- **Magnetospheric accretion columnとその根元による星のoccultation で大体説明可能ではないか。**

18.

Impact of the external radiation field on the structure and evolution of supernova remnants

Mario Romero, Yago Ascasibar, Jan Palouš, Richard Wünsch, Mercedes Mollá ★ We carry out 1D hydrodynamical simulations of the evolution of a spherically symmetric supernova remnant (SNR) subject to an external radiation field (ERF) that influences the cooling and heating rates of the gas. We consider homogeneous media with ambient hydrogen number densities $n_{\rm H,0}$ of 0.1 and 1 cm^{-3} permeated by an average radiation field including the cosmic microwave, extragalactic, and Galactic backgrounds, attenuated by an effective column density $N_{\rm H,eff}$ from 10^{18} to 10^{21} cm^{-2}. Our results may be classified into two broad categories: at low $N_{\rm H,eff}$, the ERF presents little absorption in the ultraviolet (ionising) regime, and all the 'unshielded' cases feature an equilibrium temperature $T_{eq} \sim 7000$ K below which the ambient gas cannot cool further. In this scenario, the SNR develops a nearly isothermal shock profile whose shell becomes thicker over time. At higher $N_{\rm H,eff}$, the ERF is heavily absorbed in the UV range, yielding a roughly constant heating function for temperatures $\lesssim 10^4$ K. These 'shielded' cases develop a thin, cold and dense shell throughout their evolution. Energy and momentum injection to the medium do not change significantly between both scenarios, albeit luminosity is higher and more uniformly distributed over the shell for unshielded SNR.

・SNR近傍に外部輻射場があったときにそれがSNRの構造と進化にどのような影響があるかを数値シミュレーションで調べた